Journal of Materials Chemistry B

PAPER

View Article Online
View Journal

Cite this: DOI: 10.1039/c6tb00874g

DHDMIQK(KAP): a novel nano-delivery system of dihydroxyl-tetrahydro-isoquinoline-3-carboxylic acid and KPAK towards the thrombus†

Qiqi Feng,[a] Ming Zhao,*[ab] Taiping Gan,[a] Haimei Zhu,[a] Yaonan Wang,[a] Shurui Zhao,[a] Yuji Wang,[a] Jianhui Wu[a] and Shiqi Peng*[a]

Received 8th April 2016,
Accepted 15th August 2016

DOI: 10.1039/c6tb00874g

www.rsc.org/MaterialsB

Vascular thrombosis is a major risk of the onset of stroke and so novel therapeutic candidates have been attracting interest. In this context, here docking based computer assisted screening and mesoscale simulation were used to design *N*-[(*S*)-6,7-dihydroxy-1,1-dimethyl-1,2,3,4-tetrahydroisoquinoline-3-carbonyl]-Lys(Pro-Ala-Lys), DHDMIQK(KAP), for inhibiting P-selectin expression. *In vitro*, 1 nM of DHDMIQK(KAP) effectively down-regulated P-selectin expression. In water, in rat plasma and in the solid state DHDMIQK(KAP) formed nanoparticles of a size capable of suitable delivery in the blood circulation. FT-MS and NOESY 2D NMR spectra showed DHDMIQK(KAP) formed hexamers, identified the intermolecular interactions of the hexamer, and assigned the hexamer a butterfly like conformation. Transmission electron microscopy, scanning electron microscopy and atomic force microscopy (AFM) imaged DHDMIQK(KAP) forming size-suitable nanoparticles for safe delivery in the blood circulation. In particular, AFM images showed that the nanoparticles effectively adhered onto the surfaces of the platelets. *In vivo* DHDMIQK(KAP) lysed the thrombus and inhibited thrombosis with a minimal effective dose of 0.01 nmol kg^{-1}. FT-MS spectrum analyses defined a specific distribution of DHDMIQK(KAP) in the thrombus, but not in the blood and vital organs. Therefore, DHDMIQK(KAP) should be a novel nano-delivery system of 6,7-dihydroxyl-1,2,3,4-tetrahydroisoquinoline-3-carboxylic acid and KPAK to target the thrombus.

Introduction

Vascular thrombosis is responsible for the onset of diabetes mellitus, metabolic syndrome, atherosclerosis and hypertension.[1] Blood coagulation is correlated with inflammation due to inflammation raising the risk of cardiovascular disease and damaging the haemostatic balance towards vascular thrombosis.[2] P-selectin not only mediates the rolling of blood cells on the surface of the endothelium, but also triggers the attachment of leukocytes to platelets in blood circulation, to endothelial cells and to other leukocytes at injured tissues and sites of inflammation.[3] By expressing P-selectin, platelets play a key role in inflammation and related diseases.[4,5] An increase of P-selectin expression in the lung is associated with pancreatitis.[6] Platelets of patients with coronary heart disease highly express P-selectin, and down-regulation of P-selectin expression is a potential approach to prevent and/or treat vascular thrombosis and related diseases.[7] Therefore P-selectin inhibitors are of clinical importance.

Adenosine receptor A_{2A} is widely expressed in the central nervous system, its antagonists are considered potential therapeutic agents for Parkinson's and Alzheimer's diseases.[8–10] Adenosine receptor A_{2A} can use tetrahydroisoquinoline-iminoimidazolines, the derivatives of tetrahydroisoquinoline-hydantoin, as substrates.[11] Tetrahydroisoquinolines can inhibit a series of enzymes, such as histone deacetylase,[13] anaplastic lymphoma kinase,[14] and phosphodiesterase type 4.[15] Tetra-hydroisoquinolines can also block some pathological processes, such as HIV-1 attachment,[12] inflammatory response,[18] dopamine/norepinephrine reuptake,[19] and the binding of leukocyte function-associated antigen-1 to intercellular adhesion molecule-1.[21] Besides, tetrahydroisoquinolines can antagonize some receptors and ion channels, such as the orexin 1 receptor,[16] the kappa opioid receptor,[17] and the N-type calcium channel.[20]

Of the tetrahydroisoquinolines, 1,2,3,4-tetrahydroisoquinoline-3-carboxylic acid is known as a rigid analog of Phe, which occurs as a structural block in peptide-based drugs or as an essential part of various bioactive compounds,[22] and its anti-thrombotic

[a] *Beijing Area Major Laboratory of Peptide and Small Molecular Drugs, Engineering Research Center of Endogenous Prophylactic of Ministry of Education of China, Beijing Laboratory of Biomedical Materials, College of Pharmaceutical Sciences, Capital Medical University, Beijing 100069, P. R. China.*
E-mail: mingzhao@bjmu.edu.cn, sqpeng@bjmu.edu.cn; Fax: +86-10-8391-1533; Tel: +86-10-8391-1528
[b] *Department of Biomedical Science and Environmental Biology, Kaohsiung Medical University, Kaohsiung, Taiwan*

† Electronic supplementary information (ESI) available. See DOI: 10.1039/c6tb00874g

activity can be effectively enhanced by Lys, suggesting that Lys can be used as a linking residue safely.[23] The conjugate of 1,2,3,4-tetrahydro-isoquinoline-3-carboxylic acid and RGDF can target P-selectin in particular.[24] Furthermore, 1-methyl-1,2,3,4-tetrahydroisoquinoline is an endogenous substance showing neuroprotective activity,[25] while polyphenol-rich foods possess cardiovascular protective effects.[26] With respect to peptides, Pro-Ala-Lys (PAK) is a thrombolytic active agent.[27] These findings suggest that 1,2,3,4-tetrahydroisoquinoline-3-carboxylic acid could be modified with methyl, hydroxyl and peptide, thereby leading to the rational design of a novel inhibitor of P-selectin, *N*-[(*S*)-6,7-di-hydroxy-1,1-dimethyl-1,2,3,4-tetrahydroisoquinoline-3-carbonyl]-Lys(Pro-Ala-Lys), DHDMIQK(KAP), a nano-delivery system for 6,7-dihydroxyl-1,2,3,4-tetrahydroisoquinoline-3-carboxylic acid and KPAK to treat thrombosis.[22,23,25,27]

Several polymeric nano-delivery systems, such as PPACK modified liposomes and perfluorocarbon nano-particles,[28,29] as well as multifunctional micelles,[30] are known as anti-thrombotic agents. Though these nano-delivery systems have biocompatible and biodegradable carrier materials, the carrier materials have no pharmacological activity, the amounts of the carrier materials are large in proportion to the active PPACK and CREKA, and the entities of the nano-delivery system are unable to bind receptors. In contrast to polymeric nano-delivery systems, nano-delivery DHDMIQK-(KAP) is a small molecule, KPAK and 6,7-dihydroxyl-1,2,3,4-tetra-hydroisoquinoline-3-carboxylic acid possess thrombolytic and anti-thrombotic activity, respectively, the amount of KPAK is equal in proportion to 6,7-dihydroxyl-1,2,3,4-tetrahydroisoquinoline-3-carboxylic acid, and the DHDMIQK(KAP) entity should be able to dock into the active site of P-selectin.

Fig. 1 indicates that DHDMIQK(KAP) and the amino acid residues in the active site form several hydrogen bonds, such as the hydrogen bonds formed by the two H atoms of 6,7-dihydroxyl of DHDMIQK(KAP) and the α-carboxyl oxygen of Glu88 of the active site, the hydrogen bond formed by 6-hydroxyl oxygen of DHDMIQK(KAP) and the H of the side NH_2 of Lys111 of the active site, the hydrogen bonds formed by the two H of α-NH_2 of the Pro residue of DHDMIQK(KAP) and α-carboxyl oxygen of Glu92 and Ser46 of the active site, as well as the hydrogen bond formed by the carbonyl oxygen of the Ala residue of DHDMIQK(KAP) and the phenolic hydroxyl H of Tyr94 of the active site. It is worthy of mention that these amino acid residues are in the regions of the two average structures of P-selectin,[28] and therefore DHDMIQK(KAP) may be a potential inhibitor. In this context, in the present paper we synthesized DHDMIQK(KAP), imaged its nanofeatures, evaluated its anti-thrombotic and thrombolytic activities, and examined its thrombus targeting.

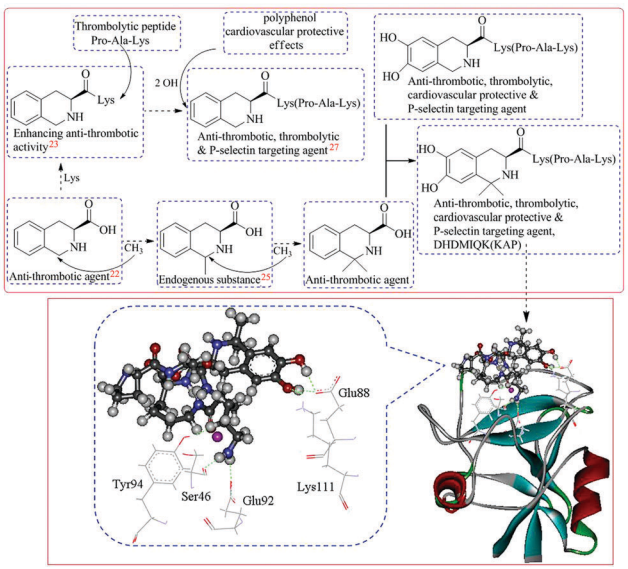

Fig. 1 Design of DHDMIQK(KAP),[22,23,25,27] and its interactions with the amino acid residues inside the active site of P-selectin.[31]

Materials and methods

General

All reagents and the protected L-amino acids were available commercially (Sigma, St Louis MO, USA). Anhydrous solvents were purified and dried by standard methods. Column chromatography was performed on silica gel of 200–300 mesh. The purities of the intermediates and the products were identified with thin layer chromatography (TLC) and high performance liquid chromatography (HPLC, C_{18} column 4.6 × 150 mm, Waters Corporation, Milford, MA, USA), and were higher than 96%. Reactions were monitored by TLC on glass plates coated with silica gel with a fluorescent indicator. Melting points were determined on an XT5 hot stage apparatus (Beijing Keyi Electro-Optic Factory, Beijing, China) and were uncorrected. Proton nuclear magnetic resonance (^{1}H NMR, 300 MHz) and ^{13}C nuclear magnetic resonance (^{13}C NMR, 75 MHz) spectra were recorded in DMSO-d_6 or $CDCl_3$, and with tetra-methylsilane as the internal standard. Electrospray ionization mass spectrometry (ESI-MS) was carried out on a ZQ 2000 (Waters Corp.) and a 9.4 T solariX Fourier transform ion cyclotron resonance mass spectrometer (FT-MS, Bruker Corp., Billerica, MA, USA), with an ESI/matrix-assisted laser desorption/ionization (MALDI) dual ion source.

Sprague Dawley rats were purchased from the Animal Center of Capital Medical University. Work performed was based on a protocol reviewed and approved by the ethics committee of Capital Medical University. The committee assures that the welfare of the animals was maintained in accordance with the requirements of the Animal Welfare Act. Statistical analyses of all biological data were carried out by use of analysis of variance. A p-value < 0.05 was considered statistically significant.

Synthesis of DHDMIQK(KAP)

The preparation of DHDMIQK(KAP) was carried out according to Scheme 1. The route consists of eight-step reactions, and the total yield was 4.1%. The details of the synthetic procedures and the physicochemical data of the intermediates and DHDMIQK(KAP) are given as follows.

Preparing (3*S*)-6,7-dihydroxy-1,1-dimethyl-1,2,3,4-tetra-hydro-isoquinoline-3-carboxylic acid (1). At 0 °C to a mixture of 5.0 g (25.0 mmol) of 3,4-dihydroxyl-L-Ph and 6.0 g (30.0 mmol) of

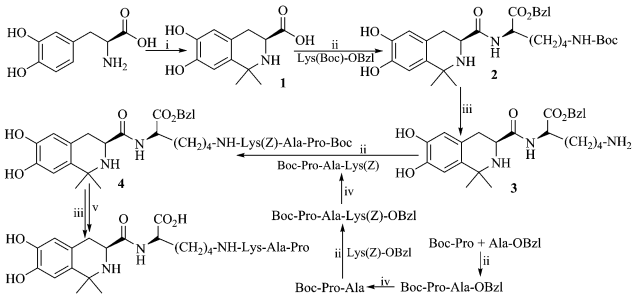

Scheme 1 Synthetic route of DHDMIQK(KAP). (i) Acetone, CF_3CO_2H, $MgSO_4$; (ii) dicyclohexylcarbodiimide (DCC), *N*-hydroxybenzotriazole (HOBt), *N*-methylmorpholine (NMM); (iii) hydrogen chloride in ethyl acetate (4 M); (iv) aqueous NaOH (2 M); (v) ethanol, Pd/C.

$MgSO_4$ in 250 mL of acetone, 25 mL of CF_3CO_2H was added, and then this reaction mixture was stirred at room temperature for 96 h. After filtration the filtrate was evaporated under vacuum. The residue was dissolved in acetone and the solution was evaporated under vacuum. This was repeated 3 times to thoroughly remove the excess CF_3CO_2H and provide 5.63 g (95%) of the title compound as a colorless powder. ESI-MS (*m*/*z*): 236 $[M - H]^-$. ^1H NMR (300 MHz, DMSO-d_6): δ/ppm = 6.61 (s, 1H), 6.45 (s, 1H), 3.70 (dd, J = 3.9, 11.4 Hz, 1H), 2.76 (dd, J = 11.7, 15.3 Hz, 1H), 2.62 (m, 1H), 1.41 (s, 3H), 1.32 (s, 3H).

Preparing *N*-[(3*S*)-6,7-dihydroxy-1,1-dimethyl-1,2,3,4-tetrahydroisoquinoline-3-carbonyl]-L-Lys(Boc)-OBzl (2). At 0 °C to a solution of 1.19 g (5.01 mmol) of (3*S*)-6,7-dihydroxy-1,1-dimethyl-1,2,3,4-tetrahydroisoquinoline-3-carboxylic acid (**1**), 1 mL (9.0 mmol) of NMM, 1.20 g (5.8 mmol) of DCC and 0.68 g (5.0 mmol) of HOBt in 20 mL of anhydrous *N*,*N*-dimethylformamide (DMF), 2.83 g (5.5 mmol) of L-Lys(Boc)-OBzl was added. This reaction mixture was stirred at 0 °C for 1 hour, then stirred at room temperature for another 6 hours, and TLC (chloroform/methanol, 15/1) indicated the complete disappearance of **1**. The reaction mixture was filtered and the filtrate was evaporated under vacuum, the residue was dissolved in 150 mL of ethyl acetate and washed successively with 5% aqueous sodium bicarbonate, 5% aqueous citric acid, and saturated aqueous sodium chloride. The ethyl acetate phase was dried over anhydrous sodium sulfate for 0.5 hours. After filtration and evaporation under vacuum, the residue was purified on a silica gel column to provide 1.63 g (59%) of the title compound as a light pink powder. ESI-MS (*m*/*z*): 556 $[M + H]^+$. ^1H NMR (300 MHz, DMSO-d_6) δ/ppm = 8.64 (s, 1H), 8.52 (s, 1H), 8.14 (d, J = 7.5 Hz, 1H), 7.36 (m, 5H), 6.74 (m, 1H), 6.57 (s, 1H), 6.37 (s, 1H), 5.14 (m, 2H), 4.30 (m, 1H), 3.55 (m, 2H), 3.32 (m, 2H), 2.88 (m, 2H), 2.57 (d, J = 3.9 Hz, 1H), 2.27 (m, 1H), 2.15 (s, 1H), 1.69 (m, 4H), 1.36 (s, 9H), 1.33 (s, 3H), 1.25 (s, 3H).

Preparing *N*-[(3*S*)-6,7-dihydroxy-1,1-dimethyl-1,2,3,4-tetra-hydroisoquinoline-3-carbonyl]-L-Lys-OBzl (3). A solution of 1.50 g (2.73 mmol) of *N*-[(3*S*)-6,7-dihydroxy-1,1-dimethyl-1,2,3,4-tetrahydroisoquinoline-3-carbonyl]-L-Lys(Boc)-OBzl (**2**) in 18 mL of ethyl acetate containing hydrogen chloride (4 M) was stirred at 0 °C for 2 hours and evaporated under vacuum. The residue was dissolved in ethyl acetate and the solution was evaporated under vacuum. This procedure was repeated 3 times to thoroughly remove the excess hydrogen chloride. The residue was triturated with ether to provide 1.02 g (82%) of the title compound as a yellow powder. ESI-MS (*m*/*z*): 456 $[M + H]^+$.

Preparing Boc-Pro-Ala-Lys(Z). By using the standard synthetic procedure of peptides the coupling of Ala-OBzl and Boc-Pro provided Boc-Pro-Ala-OBzl in 78% yield, which was treated with NaOH in methanol (2 M) at 0 °C to provide Boc-Pro-Ala in 98% yield. By using the standard synthetic procedure of peptides the coupling of Boc-Pro-Ala and Lys(Z)-OBzl provided Boc-Pro-Ala-Lys(Z)-OBzl in 76% yield (ESI-MS (*m*/*z*): 639 $[M + H]^+$), which was treated with NaOH in methanol (2 M) at 0 °C to provide Boc-Pro-Ala-Lys(Z) in 98% yield (ESI-MS (*m*/*z*): 547 $[M - H]^-$).

Preparing *N*-[(3*S*)-6,7-dihydroxy-1,1-dimethyl-1,2,3,4-tetra-hydroisoquinoline-3-carbonyl]-L-Lys[Boc-Pro-Ala-Lys(Z)]-OBzl (4). At 0 °C to a solution of 1.209 g (2.40 mmol) of Boc-Pro-Ala-Lys(Z), 0.5 mL (4.5 mmol) of NMM, 0.495 g (2.40 mmol) of DCC, 0.270 g (2.0 mmol) of HOBt and 20 mL of anhydrous DMF, 0.964 g (2.01 mmol) of *N*-[(3*S*)-6,7-dihydroxy-1,1-dimethyl-1,2,3,4-tetra-hydroisoquinoline-3-carbonyl]-L-Lys-OBzl (**3**) was added. After stirring at 0 °C for 1 hour the reaction mixture was stirred at room temperature for 6 hours, and TLC indicated the complete disappearance of **3**. The reaction mixture was filtered and the filtrate was evaporated under vacuum. The residue was dissolved in 150 mL of ethyl acetate and washed successively with 5% aqueous sodium bicarbonate, 5% aqueous citric acid, and saturated aqueous sodium chloride. The ethyl acetate phase was dried over anhydrous sodium sulfate. After filtration and evaporation under vacuum, the residue was purified on a silica gel column to provide 750 mg (38%) of the title compound as a colorless powder. ESI-MS (*m*/*z*): 987 $[M + H]^+$. ^1HNMR (300 MHz, DMSO-d_6): δ/ppm = 8.68 (s, 1H), 8.56 (s, 1H), 8.16 (m, 1H), 8.04 (m, 1H), 7.78 (m, 1H), 7.68 (m, 1H), 7.34 (m, 10H), 6.58 (s, 1H), 6.37 (s, 1H), 5.14 (s, 2H), 4.98 (s, 2H), 4.29 (m, 2H), 4.09 (m, 3H), 3.56 (m, 3H), 3.01 (m, 4H), 2.62 (m, 1H), 2.40 (m, 1H), 2.27 (m, 1H), 2.15 (s, 1H), 2.06 (m, 1H), 2.01 (s, 1H), 1.78 (m, 6H), 1.38–1.31 (m, 18H), 1.17 (m, 10H).

Preparing *N*-[(3*S*)-6,7-dihydroxy-1,1-dimethyl-1,2,3,4-tetra-hydroisoquinoline-3-carbonyl]-L-Lys(Pro-Ala-Lys) [DHD-MIQK(KAP)]. To a solution of 305 mg (0.31 mmol) of *N*-[(3*S*)-6,7-dihydroxy-1,1-dimethyl-1,2,3,4-tetra-hydroisoquinoline-3-carbonyl]-L-Lys[Boc-Pro-Ala-Lys(Z)]-OBzl (**4**) in 20 mL of ethanol, 45 mg of Pd/C was added, replacing the air of the reaction with blowing H_2 and stirring at room temperature for 8 hours. The Pd/C was removed by filtration and the filtrate was evaporated under vacuum. The resulting yellow powder was treated at 0 °C in 10 mL of ethyl acetate containing hydrogen chloride (4 M) for 2 hours. The reaction mixture was evaporated under vacuum. The residue was dissolved in ethyl acetate and the solution was evaporated under vacuum. This procedure was repeated 3 times to thoroughly remove the excess hydrogen chloride. The residue was triturated with ether to provide 152 mg (74%) of the title compound as a colorless powder. FT-MS (*m*/*z*): 662 $[M + H]^+$. M.p.: 186–188 °C. $[\alpha]_D^{25} = -1.80$ (c = 0.25, CH_3OH). IR (KBr): 3854, 3738, 2957, 2349, 2018, 1668, 1537, 1400, 1258, 1044, 872, 67 cm^{-1}. ^1H NMR (800 MHz, DMSO-d_6): δ/ppm = 10.12 (s, 1H), 9.62 (d, J = 10.4 Hz, 1H),

9.25 (t, J = 10.4 Hz, 1H), 8.96 (d, J = 7.2 Hz, 1H), 8.83 (d, J = 7.2 Hz, 1H), 8.48 (d, J = 4.8 Hz, 1H), 8.07 (m, 5H), 6.69 (s, 1H), 6.56 (s, 1H), 4.35 (m, 1H), 4.33 (m, 1H), 4.23 (m, 1H), 4.19 (m, 2H), 3.22 (m, 1H), 3.17 (m, 1H), 3.12 (m, 1H), 3.10 (m, 1H), 2.93 (m, 1H), 2.29 (m, 1H), 1.87 (m, 3H), 1.77 (m, 1H), 1.70 (m, 1H), 1.68 (s, 3H), 1.64 (m, 1H), 1.57 (m, 1H), 1.54 (s, 3H), 1.43 (m, 4H), 1.13 (m, 2H), 1.26 (d, J = 7.2 Hz, 3H). ^{13}C NMR (200 MHz, DMSO-d_6): δ/ppm = 173.30, 171.83, 171.63, 168.68, 168.27, 145.44, 145.24, 129.08, 120.48, 115.39, 112.49, 63.67, 59.07, 58.25, 52.98, 51.07, 49.21, 46.03, 42.73, 38.87, 38.57, 31.96, 30.76, 29.95, 28.99, 28.78, 27.30, 26.88, 23.98, 23.20, 22.60, 18.33.

HPLC purity of DHDMIQK(KAP)

A Waters 2695 HPLC system with a Waters 2996 PDA was used. The sample was analyzed on a Waters XTerra C_{18} reversed-phase column (column 4.6 × 150 mm, 3.5 μm; Waters Limited, Hertfordshire, UK). Onto the column, 5 μL of a solution of DHDMIQK(KAP) in acetonitrile was injected. The mobile phase was acetonitrile containing trifluoroacetic acid (0.1%). The flow rate was 1 mL minute^{-1}. The UV detector was set to a scanning range of 200–400 nm, and a wavelength of 254 nm was used to monitor DHDMIQK(KAP), of which the retention time was 5.366 minutes and the purity was 98.93% (HPLC chromatogram is shown in Fig. S5 in the ESI†).

FT-MS spectrum of DHDMIQK(KAP)

Mass spectra were recorded on a Bruker 9.4 T solariX FT-ICR mass spectrometer equipped with an ESI/MALDI dual ion source in positive and negative ion modes. Three replicate measurements were performed for each sample. Data were acquired using the solariX control software. Spectral data were processed using the Bruker Daltonics data analysis software (Bruker Corp.).

Mesoscale simulation and nanofeature prediction of DHDMIQK(KAP)

The structure of DHDMIQK(KAP) was sketched using ChemDraw Ultra 10.0 (Perkin Elmer Inc., Waltham, MA, USA) and transformed into a three-dimensional (3D) structure with Materials Studio® 3.2 (Accelrys, Inc., San Diego, CA, USA), which was optimized using the Materials Studio Forcite module. DHDMIQK(KAP) was geometry optimized until the convergence of maximum energy and maximum force changed to 2 × 10^{-5} kcal mol^{-1} and 0.001 kcal mol^{-1} Å^{-1}, respectively. A molecular dynamics simulation was performed at 500 K using the *NVT* ensemble until equilibration. The final structure was further optimized with the Materials Studio Dmol3 module. The rigid coarse grain model of DHDMIQK(KAP) was built as four connected spherical beads, based on the Dmol3 optimized structure. In a cubic box of 20 × 20 × 20 Å, the coarse grain model of DHDMIQK(KAP) was randomly distributed with a density of 0.15 g cm^{-3}. A 15 000 ps simulation was performed on this system at 298 K using the *NVT* ensemble.

NOESY 2D NMR spectra of DHDMIQK(KAP)

^{1}H NMR and NOESY 2D NMR spectra were recorded on a Bruker 800 MHz spectrometer with DMSO-d_6 as the solvent and tetra-methylsilane as the internal standard.

Measuring particle size of DHDMIQK(KAP) in water

To characterize DHDMIQK(KAP) in ultrapure water, the particle size of DHDMIQK(KAP) in water (10^{-11}, 10^{-9} and 10^{-7} M) was determined on a particle size analyzer (Nano-ZS90; Malvern Instruments Ltd, Malvern, UK). The particle size was measured at 25 °C.

Transmission electron microscopy of DHDMIQK(KAP)

DHDMIQK(KAP) in ultrapure water was characterized by transmission electron microscopy (TEM, JSM-6360 LV; JEOL, Tokyo, Japan). The solution of DHDM-IQK(KAP) in ultrapure water (10^{-11}, 10^{-9} and 10^{-7} M) was dripped onto a carbon-coated formvar copper grid. The grid was dried thoroughly in air, and the TEM image was recorded at 80 kV electron beam accelerating voltage. The nano-images were recorded on an imaging plate (Gatan Bioscan camera model 1792) with 20 eV energy windows at 6000–400 000×. The TEM image was obtained from counting over 100 species in a randomly selected region. The images were digitally enlarged. All determinations were carried out in triplicate grids.

Scanning electron microscopy of DHDMIQK(KAP)

The shape and size of the nanospecies of lyophilized powders from a solution of DHDMIQK(KAP) in ultrapure water were measured by scanning electron microscopy (SEM, JEM-1230; JEOL) at 50 kV. The powders were attached to a copper plate with double-sided tape (Euromedex, Souffelweyersheim, France). The specimens were coated with 20 nm gold–palladium using a JEOL JFC-1600 Auto Fine Coater. The coater was operated at 15 kV, 30 mA, and 200 mTorr (argon) for 60 seconds. The shape and size distributions of the nanoparticles were measured by examining 100 particles in randomly selected regions on the SEM alloy. All measurements were performed on triplicate grids. Images were recorded on an imaging plate (Gatan Bioscan Camera Model 1792; Gatan, Inc.) with 20 eV energy windows at 100–10 000×, and they were digitally enlarged.

Atomic force microscopy (AFM) of DHDMIQK(KAP)

The contact mode atomic force microscopy (AFM) test was carried out using a Nanoscope 3D AFM (Veeco Instruments Ltd, Plainview, NY, USA) to visualize the 3D morphological characteristics of DHDMIQK(KAP) in rat blood. The images of rat plasma alone (negative control) and DHDMIQK(KAP) in aqueous solution (positive control, 10^{-11} M, 10^{-9} M and 10^{-7} M, pH 7.4) were also recorded.

AFM imaging visualizing the interaction of DHDMIQK(KAP) with rat platelets

Rat blood containing 3.8% sodium citrate (1 : 9 v/v, citrate : blood) was centrifuged at 100g for 10 min, and the platelet-rich plasma (PRP) was collected. Then PRP was centrifuged for an additional 10 min at 300g to collect the precipitates, to which 1.5 mL of normal saline (NS) was added, mixed and centrifuged (300g, 10 min) to get normal platelets of 1 × 10^5 cells per mL concentration as a NS control sample. Normal platelets of

1×10^5 cells per mL concentration were incubated with DHDMIQK(KAP) (final concentration, 1×10^{-9} μM) at 37 °C for 30 min as a treatment control sample. Normal platelets of 1×10^5 cells per mL concentration were activated with arachidonic acid (AA, Sigma-Aldrich Co., final concentration 350 μM) at 37 °C for 5 min to obtain an AA activated sample. AA activated platelets of 1×10^5 cells per mL concentration were incubated with DHDMIQK(KAP) (final concentration, 1×10^{-9} μM) at 37 °C for 30 min as the treatment sample. The samples were individually dropped onto a mica sheet, fixed with glutaraldehyde (3%) for 10 min, carefully washed with ultrapure water, and dried in air.

Testing the Faraday–Tyndall effect and nano-properties of DHDMIQK(KAP) in water

To explore the nano-properties of aqueous DHDMIQK(KAP), the Faraday–Tyndall effect was tested. The solution of DHDMIQK(KAP) in ultrapure water (1 nM, pH 7.0) was irradiated with a laser beam at 650 nm. In addition, the zeta potentials were determined on a Malvern Zetasizer (Nano-ZS90; Malvern Instruments) with the DTS (Nano) Program.

In vitro antiplatelet aggregation assay of DHDMIQK(KAP)

A two-channel chronolog aggregometer was used to evaluate platelet aggregation. The platelet count was determined with an H-10 cell counter. Pig blood containing 3.8% sodium citrate (1 : 9 v/v, citrate : blood; purchased from the Laboratory Animal Center of Capital Medical University) was centrifuged at 100*g* for 10 minutes, and the platelet-rich plasma (PRP) was collected. The remaining blood was centrifuged for an additional 10 minutes at 1500*g* to prepare platelet-poor plasma. The final platelet count of the PRP was adjusted to 2×10^8 platelets per mL with autologous platelet-poor plasma. Into an optical aggregometry testing tube, 0.5 mL of the adjusted plasma sample and 5 μL of NS, or 5 μL of the solution of DHDMIQK(KAP) in NS (in a series of final concentrations of 10, 1, 0.1, 0.05 and 0.01 mg mL^{-1}) was added. After adjusting the baseline, 5 μL of a solution of platelet-activating factor (PAF, Sigma-Aldrich Co.) in NS (final concentration 0.1 μM), or 5 μL of a solution of adenosine diphosphate (ADP, Sigma-Aldrich Co.) in NS (final concentration 10 μM), or 5 μL of a solution of AA in NS (final concentration 350 μM), or 5 μL of a solution of thrombin (TH, Sigma-Aldrich Co.) in NS (final concentration 0.5 U mL^{-1}) was added, and aggregation was recorded at 37 °C for 5 minutes. The effect of DHDMIQK(KAP), *N*-[(3*S*)-6,7-dihydroxy-1,1-dimethyl-1,2,3,4-tetrahydroisoquinoline-3-carbonyl]-L-Lys (DHDMIQ), and Lys-Pro-Ala-Lys (KPAK) on PAF, ADP, AA or TH induced platelet aggregation was observed. Six replicates were performed. The maximum platelet aggregation (A_m) of NS, DHDMIQ, KPAK or DHDMIQK(KAP) was represented by the peak height of the aggregation curve (equals the maximum light transmission). The inhibition rate was calculated according to inhibition% = (1 − [A_m% of DHDMIQK(KAP)/A_m% of NS]) × 100%. The concentration *vs.* inhibition rate curve was plotted to determine the values of half maximal inhibitory concentration (IC_{50}) with the statistical program GWBASIC.EXE (GWBASIC is a dialect of the BASIC programming language developed by Microsoft Corporation [Redmond, WA, USA] from BASICA).

P-selectin enzyme-linked immunosorbent assay of DHDMIQK(KAP)

Into a syringe containing 500 μL of 3.8% sodium citrate (anticoagulant), 4500 μL of blood from the carotid of an anesthetized rat was collected and centrifuged at 200*g* for 20 minutes to collect the plasma. To 960 μL of the plasma, 20 μL of DHDMIQK(KAP), DHDMIQ and KPAK in NS (10^{-9} M) or 20 μL of NS was added. The reaction mixtures were incubated at 37 °C for 10 min, then 20 μL of AA in NS (0.15 g L^{-1}) was added and incubated for another 5 min. The plate was treated according to the manufacturer's instructions (rat P-selectin enzyme-linked immunosorbent assay kit; RAPID West Hills, CA, USA). The optical density (OD) value of each well was tested at 450 nm and the P-selectin level was calculated according to the standard samples from the kit.

ESR assay of DHDMIQK(KAP) in scavenging NO•

The signals of NO• free radicals, which were produced by the reaction of 5 μL of a solution of 7.325 mg of *N*-methyl-D-glucamine dithiocarbamate (MGD, Sigma-Aldrich Co.) in 1 mL ultrapure water (25 mM), 5 μL of a solution of 3.475 g of $FeSO_4 \cdot 7H_2O$ (Sinopharm Chemical Reagent Beijing Co., Ltd, Beijing, China) in 1 mL ultrapure water (12.5 mM) and 5 μL of a solution of 0.25 mg of *S*-nitroso-*N*-acetyl-DL-penicillamine (SNAP, Sigma-Aldrich Co.) in 1 mL ultrapure water (1.1 μM), were measured on a JEOL JES300ESR. The height of the signal was calculated and defined as the blank height of the NO• signal (BHNO). The effect of DHDMIQK(KAP), DHDMIQ and KPAK on the level of NO• free radicals was measured by the signal of NO• free radicals formed from the reaction of 5 μL of a solution of 7.325 mg of MGD in 1 mL ultrapure water (25 mM), 5 μL of a solution of 3.475 g of $FeSO_4 \cdot 7H_2O$ in 1 mL ultrapure water (12.5 mM), 5 μL of a solution of 0.25 mg of SNAP in 1 mL ultrapure water (1.1 μM), and 5 μL of a solution of DHDMIQK(KAP), DHDMIQ or KPAK in 1 mL ultrapure water (every final concentration: 1×10^{-5}, 5×10^{-5}, 1×10^{-4}, 5×10^{-4} and 1×10^{-3} M). The height of the signal was calculated and defined as the DHDMIQK(KAP)-treated, DHDMIQ-treated and KPAK-treated height of the NO• signal, respectively (THNO). The NO• scavenging ratio was calculated according to 'Scavenging ratio = (BHNO• − THNO•)/BHNO•'. The concentration *vs.* scavenging ratio rate curve was plotted to determine the IC_{50} values with the statistical program GWBASIC.EXE (GWBASIC is a dialect of the BASIC programming language developed by Microsoft Corporation [Redmond, WA, USA] from BASICA).

ESR assay of DHDMIQK(KAP) in scavenging $^{\bullet}O_2^-$

The signals of $^{\bullet}O_2^-$ free radicals, which were produced by the reaction of 5 μL of a solution of 11.316 mg of dimethylpyridine *N*-oxide (DMPO, Sigma-Aldrich Co.) in 1 mL ultrapure water (0.1 M), 5 μL of a solution of diethylenetriamine pentaacetic acid (DETAPAC, Sigma-Aldrich Co.) in ultrapure water (0.9 mM), 5 μL of a solution of 0.3 g of xanthine (Sigma-Aldrich Co.) in 1 mL ultrapure water (0.5 M) and 5 μL of a solution of commercial xanthine oxidase (Sigma-Aldrich Co.) diluted by ultrapure water (1/10, v/v), were measured on a JEOL JES300ESR. The height of the signal was calculated and defined as the blank height of the

$^{\bullet}O_2^-$ signal ($BH{\cdot}O_2^-$). The effect of DHDM-IQK(KAP), DHDMIQ and KPAK on the level of $^{\bullet}O_2^-$ free radicals was measured by the signal of $^{\bullet}O_2^-$ free radicals formed from the reaction of 5 μL of a solution of 11.316 mg of DMPO in 1 mL ultrapure water (0.1 M), 5 μL of a solution of DETAPAC in ultrapure water (0.9 mM), 5 μL of a solution of 0.3 g of xanthine in 1 mL of ultrapure water (0.5 M), 5 μL of a solution of commercial xanthine oxidase diluted by ultrapure water (1/10, v/v), and 5 μL of a solution of DHDM-IQK(KAP), DHDMIQ or KPAK in 1 mL of ultrapure water (final concentrations: 1×10^{-5}, 5×10^{-5}, 1×10^{-4}, 5×10^{-4} and 1×10^{-3} M). The height of the signal was calculated and defined as the DHDMIQK(KAP)-treated, DHDMIQ-treated and KPAK-treated height of the $^{\bullet}O_2^-$ signal, respectively ($TH{\cdot}O_2^-$). The $^{\bullet}O_2^-$ scavenging ratio was calculated according to 'Scavenging ratio = $(BH{\cdot}O_2^- - TH{\cdot}O_2^-)/BH{\cdot}O_2^-$'. The concentration *vs.* scavenging ratio rate curve was plotted to determine the IC_{50} values with the statistical program GWBASIC.EXE (GWBASIC is a dialect of the BASIC programming language developed by Microsoft Corporation [Redmond, WA, USA] from BASICA).

ESR assay of DHDMIQK(KAP) in scavenging $^{\bullet}OH$

The signals of $^{\bullet}OH$ free radicals, which were produced by the reaction of 2.5 μL of a solution of 2.78 g of $FeSO_4{\cdot}7H_2O$ in 1 mL ultrapure water (10 mM), 2.5 μL of a solution of 11.32 mg of DMPO in 1 mL ultrapure water (0.1 M) and 5 μL H_2O_2 (Sinopharm Chemical Reagent Beijing Co., Ltd; 100 mM), were measured on a JEOL JES300ESR. The height of the signal was calculated and defined as the blank height of the $^{\bullet}OH$ signal ($BH{\cdot}OH$). The effect of DHDMIQK(KAP), DHDMIQ and KPAK on the level of $^{\bullet}OH$ free radicals was measured by the signal of $^{\bullet}OH$ free radicals formed from the reaction of 2.5 μL of a solution of 2.78 g of $FeSO_4{\cdot}7H_2O$ in 1 mL ultrapure water (10 mM), 2.5 μL of a solution of 11.32 mg of DMPO in 1 mL ultrapure water (0.1 M), 5 μL H_2O_2 (100 mM) and 5 μL of a solution of DHDMIQK(KAP), DHDMIQ or KPAK in 1 mL ultrapure water (every final concentration: 1×10^{-5}, 5×10^{-5}, 1×10^{-4}, 5×10^{-4} and 1×10^{-3} M). The height of the signal was calculated and defined as the DHDMIQK(KAP)-treated, DHDMIQ-treated and KPAK-treated height of the $^{\bullet}OH$ signal, respectively ($TH{\cdot}OH$). The $^{\bullet}OH$ scavenging ratio was calculated according to 'Scavenging ratio = $(BH{\cdot}OH - TH{\cdot}OH)/BH{\cdot}OH$'. The concentration *vs.* scavenging ratio rate curve was plotted to determine the IC_{50} values with the statistical program GWBASIC.EXE (GWBASIC is a dialect of the BASIC programming language developed by Microsoft Corporation [Redmond, WA, USA] from BASICA).

In vivo thrombolytic assay of DHDMIQK(KAP)

Male Wistar rats weighing 200–220 g (purchased from the Animal Center of Capital Medical University) were anesthetized with pentobarbital sodium (80.0 mg kg^{-1}, intraperitoneal). The right carotid artery and left vein jugular of the animals were separated. To a glass tube filled with artery blood (~0.1 mL) obtained from the right carotid artery of the animal, a stainless steel filament helix (15 circles, 16 mm in length, 1.0 mm in diameter) was put in immediately. After 40 minutes the helix with thrombus was carefully taken out, weighed and put into a polyethylene tube. The polyethylene tube was filled with heparin sodium (50 IU mL^{-1} in NS) and one end was inserted into the left jugular vein. Heparin sodium was injected *via* the other end of the polyethylene tube as the anticoagulant, and this end was inserted into the right carotid artery, following which 3 mL kg^{-1} of NS, DHDMIQK(KAP) in NS (0.1, 0.01, 0.001 nmol kg^{-1}), DHDMIQ and KPAK (0.1 nmol kg^{-1}) in NS, or urokinase (UK) in NS (20 000 IU kg^{-1}) was injected. The blood was circulated through the polyethylene tube for 60 minutes, after which the helix was taken out to record weight. The reduction of thrombus weight was calculated to represent the activity.

In vivo antithrombotic assay of DHDMIQK(KAP)

Male Wistar rats weighing 200–220 g were used in this assay. Aspirin (positive control) and DHDMIQK(KAP) were dissolved in NS before administration. Thirty minutes after the oral administration of 3 mL kg^{-1} of aspirin in NS (167 μmol kg^{-1} and 16.7 μmol kg^{-1}), the rats were anesthetized with pento-barbital sodium (Beijing Pharmaceutical Works, 80.0 mg kg^{-1}, intraperitoneal) and the right carotid artery and left jugular vein were separated. A weighted thread of 6 cm in length was inserted into the middle of a polyethylene tube which was filled with heparin sodium (50 IU mL^{-1}, in NS). One end of the polyethylene tube was inserted into the left jugular vein. From the other end of the polyethylene tube, heparin sodium was injected as anticoagulant, and this end was inserted into the right carotid artery. Blood was allowed to flow from the right carotid artery to the left jugular vein through the polyethylene tube for 15 minutes. The thread was retrieved to obtain the thrombus weight.

The intravenous administration of 3 mL kg^{-1} of NS (negative control), 3 mL kg^{-1} of DHDMIQK(KAP) in NS (0.1, 0.01 and 0.001 nmol kg^{-1}), DHDMIQ and KPAK in NS (0.1 nmol kg^{-1}) was carried out momentarily after the polyethylene tube was inserted into the right carotid artery. Blood was allowed to flow from the right carotid artery to the left jugular vein through the polyethylene tube for 15 minutes. The thread was retrieved to obtain the thrombus weight.

Distribution of DHDMIQK(KAP) in thrombus and vital organs

To estimate the distribution of DHDMIQK(KAP), the brain, heart, spleen, liver, kidney, lung, blood and thrombus from rats undergoing the *in vivo* antithrombotic assay, in which the rats were treated with NS or 100 nmol kg^{-1} of DHDMIQK(KAP), were homogenized, ultrasonically extracted with methyl alcohol, and centrifuged at 1000*g* for 10 minutes to separate the supernatant for ESI(±)-MS tests.

Results and discussion

FT-MS spectra and DHDMIQK(KAP)'s hexamer

The FT-MS spectrum of DHDMIQK(KAP) in ultrapure water is shown in Fig. 2A. The spectrum gives a positive ion peak of $[M + H]^{2+}$ at 1986.17767 of the mass of a hexamer plus H, a positive ion peak of $[M + H]^{2+}$ at 1654.47219 of the mass of a pentamer plus H, a positive ion peak of $[M + H]^{+}$ at 1985.18013

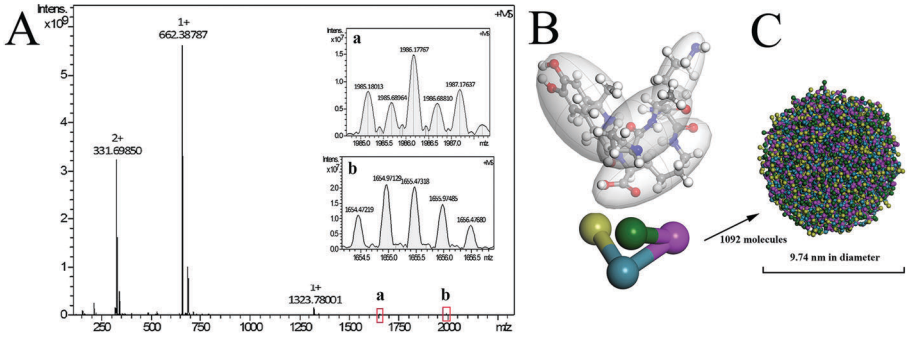

Fig. 2 FT-MS spectrum and the amplified peaks of the hexamer, in which inset (a) represents the peak of the hexamer at 1986.17767 and inset (b) represents the pentamer at 1654.47219 (A), mesoscale simulation (B), and the number of DHDMIQK(KAP) monomers in a mesoscale simulation predicted nanoparticle of 9.74 nm in diameter (C).

of the mass of a trimer plus H, a positive ion peak of $[M + H]^+$ at 1323.78001 of the mass of a dimer plus H, and a positive ion peak of $[M + H]^+$ at 662.38787 of the mass of a monomer plus H.

The qCID spectra (Fig. S6 in ESI†) indicate that the pentamer, trimer, dimer and monomer are the fragmentation products of the hexamer. Therefore the hexamer is the sole existing form of DHDMIQK(KAP) in water. It is noticed that the FT-MS spectrum gives no ion peak of a tetramer. This means that in the positive ion mode of ESI/MALDI the tetramer ion of DHDMIQK(KAP) is unstable.

NOESY spectrum and the manner of DHDMIQK(KAP) forming hexamer

To show the intermolecular association pattern the NOESY 2D NMR spectrum of DHDMIQK(KAP) was recorded with the standard method and is shown in Fig. 3A. Two interesting cross-peaks are given. Cross-peak 1 results from the interaction of amide H of the Pro residue of the PAK chain of one molecule with the H on the 3-position of the isoquinoline residue of another molecule, and cross-peak 2 results from the interaction of aromatic H of the isoquinoline residue of one molecule with the cyclic H on the 5-position of the Pro residue of the PAK chain of another molecule, suggesting the distances between the isoquinoline residues of one molecule and the Pro residues in the PAK chain of another molecule are less than 4 Å.

A three-step procedure was used to clarify the butterfly-like conformation of DHDMIQK(KAP)'s hexamer. Firstly, the energy minimized 3D structure of DHDMIQK(KAP) was used as its monomer. Secondly, the two cross-peaks were used to define the approaching manner of the 3D structure of DHDMIQK(KAP). Finally, six monomers having the energy minimized 3D structure were packed together by following the approaching manner defined by the two cross-peaks to provide a butterfly like conformation of the hexamer (Fig. 3B).

Mesoscale simulated nanostructure of DHDMIQK(KAP)

To predict their nanostructure, DHDMIQK(KAP) molecules are built and optimized simply in the Visualizer window. "Beads" are constructed from atomistic simulations and placed at the center-of-mass of groups of atoms corresponding to the particular parts of the DHDMIQK(KAP) molecule (Fig. 2B). The mesoscale simulation software assisted calculation shows that, employing the monomer as a building block, 1092 monomers can form a nanoparticle of 9.74 nm in diameter (Fig. 2C).

Nanospecies' size distribution and concentration dependent particle size

The nanospecies size distributions at 10^{-11} M, 10^{-9} M and 10^{-7} M of DHDMIQK(KAP) in ultrapure water were explored

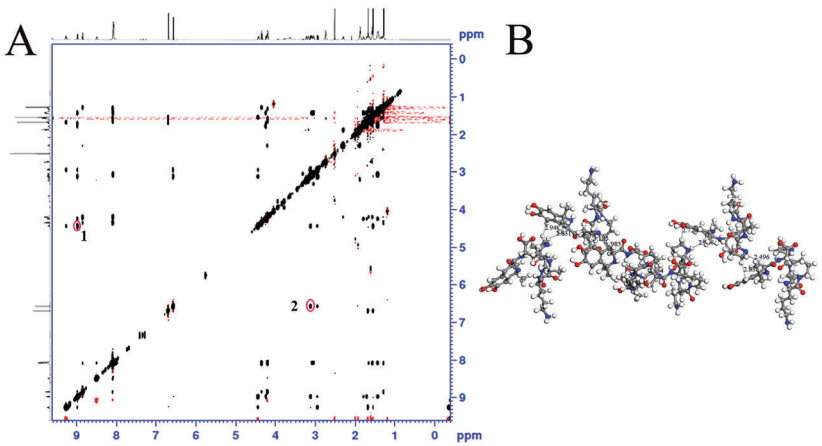

Fig. 3 NOESY 2D NMR spectrum (A) and butterfly-like conformation of DHDMIQK(KAP)'s hexamer (B).

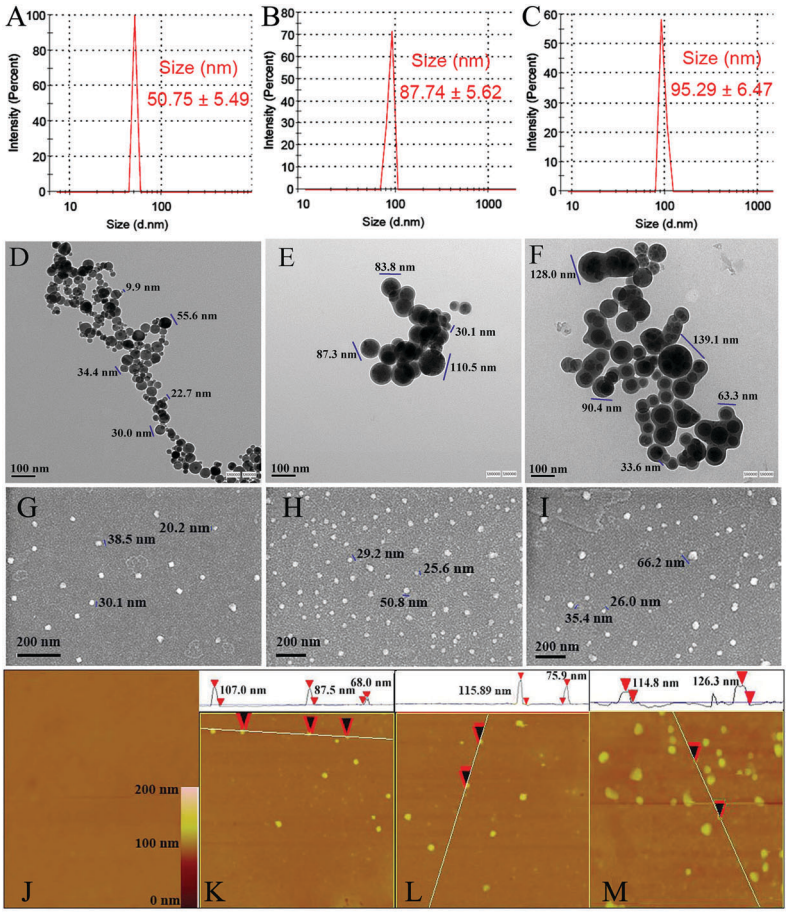

Fig. 4 Particle size analyzer defined size distribution of DHDMIQK(KAP) in 10^{-11} M (A), 10^{-9} M (B) and 10^{-7} M (C) aqueous solutions; TEM images and diameters of the nanoparticles of DHDMIQK(KAP) formed in 10^{-11} M (D), 10^{-9} M (E) and 10^{-7} M (F) aqueous solutions; SEM images and diameters of DHDMIQK(KAP)'s solids from 10^{-11} M (G), 10^{-9} M (H) and 10^{-7} M (I) aqueous solutions; AFM images of rat plasma alone (J), and DHDMIQK(KAP) in rat plasma at 10^{-11} M (K), 10^{-9} M (L) and 10^{-7} M (M).

with a particle size analyzer and are shown in Fig. 4. The size distributions of Fig. 4A, B and C are 50.75 ± 5.49 nm, 87.74 ± 5.62 nm, and 95.29 ± 6.47 nm, respectively, suggesting the average diameters of the nanoparticles progressively increase as the concentration of the solution increases from 10^{-11} M to 10^{-7} M, suggesting the nanospecies' size distribution depends on the concentration.

TEM image and concentration dependent particle size

The nanofeatures and nanospecies size of 10^{-11} M, 10^{-9} M and 10^{-7} M solutions of DHDMIQK(KAP) in ultrapure water were explored with TEM images. Fig. 4D, E and F indicate that in 10^{-11} M, 10^{-9} M and 10^{-7} M aqueous solutions DHDMIQK(KAP) forms nanoparticles of 9.9–55.6 nm in diameter, 30.1–110.5 nm in diameter and 33.6–139.1 nm in diameter, respectively. Thus as the concentration increased from 10^{-11} M to 10^{-7} M the diameter of the nanoparticles progressively increased, suggesting that the particle size depends on the concentration. Besides, there is a nanoparticle of 9.9 nm in diameter in Fig. 4D, which is close to the 9.74 nm diameter of the mesoscale simulated nanoparticle. According to the mesoscale simulation, the nanoparticle of 9.9 nm in diameter in Fig. 4D should contain 1092 monomers of DHDMIQK(KAP).

SEM image and concentration dependent solids size

The nanofeatures and nanospecies size of DHDMIQK(KAP) in the solid state were explored with SEM images. The nanofeatures of the solids from 10^{-11} M, 10^{-9} M and 10^{-7} M aqueous solutions of DHDMIQK(KAP) are also shown in Fig. 4. Fig. 4G, H and I indicate that the solids formed from 10^{-11} M, 10^{-9} M and 10^{-7} M aqueous solutions of DHDMIQK(KAP) are nanoparticles of 20.2–38.5 nm in diameter, 29.2–50.8 nm in diameter and 26.0–66.2 nm in diameter, respectively. The data show that, as the concentration of the mother solution of the solids increased from 10^{-11} M to 10^{-7} M, their diameter progressively increases, suggesting the size of the solids depends on the concentration of the mother solution.

AFM image and concentration dependent particle size

The nanofeatures and nanospecies size of DHDMIQK(KAP) in rat plasma at concentrations of 10^{-11} M, 10^{-9} M and 10^{-7} M were explored with AFM images, and are again shown in Fig. 4.

Fig. 4J indicates that rat plasma alone gives no particles. Fig. 4K, L and M indicate that, in rat plasma, 10^{-11} M, 10^{-9} M and 10^{-7} M concentrations of DHDMIQK(KAP) form nanoparticles of 68.0–107.0 nm in height, 75.9–115.9 nm in height and 114.8–126.3 nm in height, respectively. Thus as the concentration of DHDMIQK(KAP) in rat plasma increases from 10^{-11} M to 10^{-7} M the size of the nanoparticles progressively increases, suggesting particle size depends on the concentration. In addition, the sizes of most nanoparticles are close to 100 nm in height. Therefore the nanospecies size distributions, the TEM images, SEM images and AFM images consistently show that the nanoparticle size of DHDMIQK(KAP) in water, in solid state and in rat blood depends on the concentration. The nanoparticle size of DHDMIQK(KAP) in blood of close to 100 nm in height implies that the nanoparticles would not be phagocytized by macrophages and DHDMIQK(KAP) can safely deliver in blood circulation.[32]

Nano-properties of DHDMIQK(KAP)'s aqueous solution

The nano-properties of DHDMIQK(KAP)'s aqueous solution were characterized by the Faraday–Tyndall effect and zeta potential. Fig. 5A and C indicate that, with and without irradiation with a 650 nm laser beam, ultrapure water alone gives no Faraday–Tyndall effect. Fig. 5B indicates that without irradiation with a 650 nm laser beam a 1 nM solution of DHDMIQK(KAP) in ultrapure water also gives no Faraday–Tyndall effect. Fig. 5D indicates that the irradiation of a 650 nm laser beam induces a 1 nM solution of DHDMIQK(KAP) in ultrapure water, a clean solution rather than a liposomes and micelles like colloid solution, to show the Faraday–Tyndall effect. Thus the Faraday–Tyndall effect demonstrates that a 1 nM solution of DHDMIQK(KAP) in ultrapure water possesses nano-properties. The nano-properties of this solution were also characterized using zeta potential. Fig. 5E shows that the zeta potential of a 1 nM solution of DHDMIQK(KAP) in ultrapure water is −9.82 mV, and the half width of the peak is 4.20 mV. Thus the Faraday–Tyndall effect and zeta potential consistently support that the solution of DHDMIQK(KAP) in ultrapure water is a nano-solution.

In vitro activities of DHDMIQK(KAP)

The *in vitro* activities of DHDMIQK(KAP) were evaluated with an anti-platelet aggregation assay, P-selectin enzyme-linked immunosorbent assay and free radical scavenging assay. The anti-platelet aggregation assay explored the *in vitro* activities of DHDMIQK(KAP) inhibiting TH, AA, ADP and PAF induced platelet aggregations, which are represented with IC_{50} values and are shown in Fig. 6A. In respect of the IC_{50} values of DHDMIQK(KAP) inhibiting four aggregators-induced platelet aggregations, TH and PAF are the most sensitive aggregators to DHDMIQK(KAP), while AA is the most insensitive aggregator to DHDMIQK(KAP). On the other hand, the IC_{50} values of KPAK inhibiting TH, AA, ADP and PAF induced platelet aggregations are higher than 1000 nM. Since the IC_{50} values range from 2.1 μM to 16.3 μM, DHDMIQK(KAP) should be considered an effective inhibitor for the four aggregators *in vitro*.

The P-selectin enzyme-linked immunosorbent assay explored the *in vitro* activities of NS and DHDMIQK(KAP) in regulating the expression of P-selectin by AA-activated rat platelets and the data are shown in Fig. 6B. As can be seen, compared to the expression of P-selectin by AA-activated rat platelets treated with NS, 1 nM of DHDMIQK(KAP) leads to a ∼50% decrease in the expression of P-selectin. On the other hand, KPAK exhibits no such activity. It is well known that P-selectin can be translocated from the α-granules to the surface of activated platelets. In the aggregation of platelets and PSGL-1 (CD162) bearing cells the

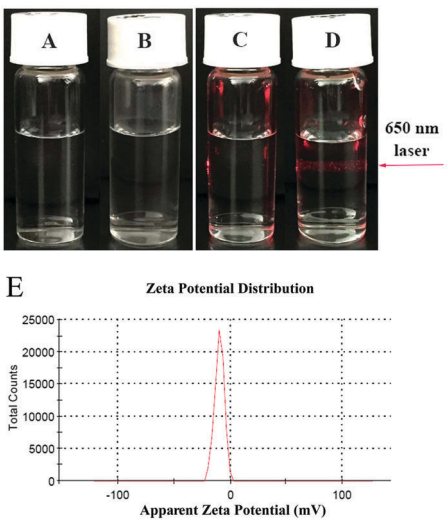

Fig. 5 Faraday–Tyndall effect and zeta potential of DHDMIQK-(KAP)'s aqueous solution at 1 nM. (A) Ultrapure water alone without radiation; (B) DHDMIQK(KAP) in ultrapure water without radiation; (C) ultrapure water alone with 650 nm laser radiation; (D) DHDMIQK(KAP) in ultrapure water with 650 nm laser radiation; (E) zeta potential of DHDMIQK(KAP) in ultrapure water.

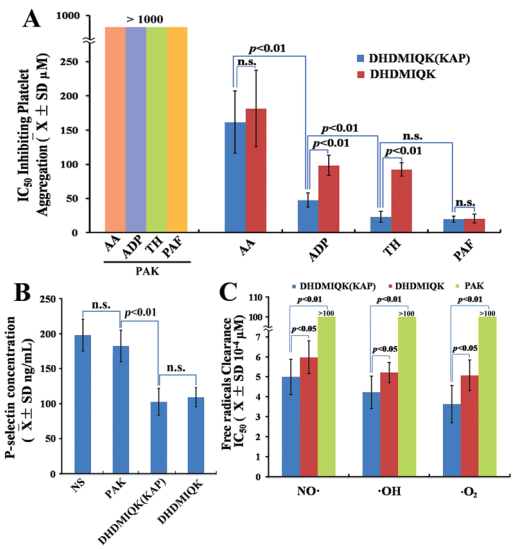

Fig. 6 *In vitro* activities of DHDMIQK(KAP), n = 6. (A) IC_{50} values of DHDMIQK(KAP) inhibiting TH, AA, ADP, and PAF induced platelet aggregation; (B) the expression of AA-activated rat platelets treated with 1 nM of DHDMIQK(KAP); (C) IC_{50} values of DHDMIQK(KAP) in scavenging NO•, $•O_2^-$ and •OH free radicals.

up-regulation of P-selectin plays an important role.[33] Thus it should be reasonable that, *via* down-regulating the expression of P-selectin, DHDMIQK(KAP) effectively inhibits platelet aggregation.

The free radical scavenging assay explored the *in vitro* activities of DHDMIQK(KAP) in scavenging NO•, $^{\bullet}O_2^-$ and •OH free radicals, which are represented with IC_{50} values (shown in Fig. 6C) and these are 499 ± 89 pM, 363 ± 94 pM and 422 ± 82 pM, respectively. Thus for the three free radicals, DHDMIQK(KAP) exhibits a similar scavenging efficacy. It is well known that the inhibition of H_2O_2 abrogates P-selectin up-regulation,[34] and NO• produced by platelets acts as a negative feedback mechanism to inhibit platelet aggregation and platelet recruitment.[35] This means that *via* scavenging NO•, $^{\bullet}O_2^-$ and •OH free radicals DHDMIQK(KAP) down-regulates the expression of P-selectin and thereby inhibits platelet aggregation.

In vivo activities of DHDMIQK(KAP)

The *in vivo* activities of DHDMIQK(KAP) were evaluated in thrombolytic and anti-thrombotic rat models. The thrombolytic efficacy of DHDMIQK(KAP) *in vivo* is represented by the reduction of thrombus weight. Fig. 7A indicates that the reductions of thrombus weights of the rats receiving 0.1, 0.01 and 0.001 nmol kg^{-1} of DHDMIQK(KAP) are 21.61 ± 4.62 mg, 14.62 ± 2.46 mg and 11.73 ± 2.15 mg, respectively, reflecting a dose dependent action. Besides, the reduction of thrombus weight of the rats receiving 0.001 nmol kg^{-1} of DHDMIQK(KAP) is not significantly different from that of the rats receiving NS ($p > 0.05$), and the reduction of thrombus weight of the rats receiving 0.1 nmol kg^{-1} of DHDMIQK(KAP) is not significantly different from that of the rats receiving 20 000 UI kg^{-1} of UK ($p > 0.05$). Therefore the minimal effective dose of DHDMIQK(KAP) for lysing a thrombus is 0.01 nmol kg^{-1} and the thrombolytic efficacy of 0.1 nmol kg^{-1} of DHDMIQK(KAP) is equal to that of 20 000 UI kg^{-1} of UK. Though KPAK is a thrombolytic agent, its thrombolytic activity at a dose of 10 μmol kg^{-1} is equal to that of 20 000 UI kg^{-1} UK.[36] The comparison of the doses/thrombolytic activities leads to an understanding that at 1/100 000 of KPAK's dose DHDMIQK(KAP) is able to exhibit a similar activity. This dramatic dose/activity difference between DHDMIQK(KAP) and PAK emphasizes that the thrombolytic action of DHDMIQK(KAP) results from the whole molecule, not the KPAK moiety.

The anti-thrombotic efficacy of DHDMIQK(KAP) *in vivo* is represented by the thrombus weight. Fig. 7B indicates that the thrombus weights of the rats treated with 0.1, 0.01 and 0.001 nmol kg^{-1} of DHDMIQK(KAP) are 52.16 ± 2.02 mg, 57.34 ± 3.73 mg and 61.91 ± 3.27 mg, respectively, reflecting a dose dependent action. The thrombus weight of the rats treated with 0.001 nmol kg^{-1} of DHDMIQK(KAP) is close to that of the rats treated with NS (63.46 ± 3.67 mg, $p > 0.05$) and 16.7 μmol kg^{-1} of aspirin (63.46 ± 4.80 mg, $p > 0.05$). Thus the minimal effective dose of DHDMIQK(KAP) is 0.01 nmol kg^{-1}, and this equals 1/16 700 000 of the dose of aspirin. Therefore DHDMIQK(KAP) is an excellent anti-thrombotic agent.

It is well known that free radicals trigger the pathogenesis of arterial and venous stroke,[37] decreasing the generation of free radicals significantly reduces the risk of thrombosis,[38] down-regulating P-selectin expression decreases thrombus burden,[39] and introducing Lys into 1,2,3,4-tetra-hydroisoquinoline-3-carboxylic acid enhances the anti-thrombotic activity.[23] Therefore the high thrombolytic and anti-thrombotic activities of DHDMIQK(KAP) should be the result of a combination of the influence of these four factors.

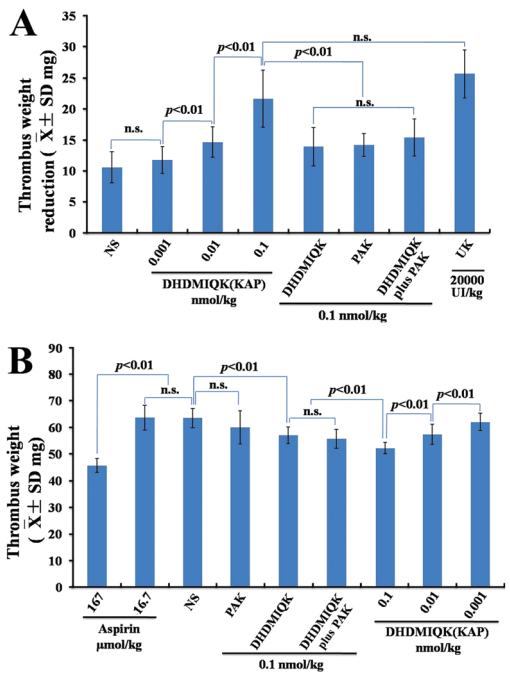

Fig. 7 *In vivo* activities of DHDMIQK(KAP), n = 12. Dose dependent thrombolytic action (A) and anti-thrombotic action (B) of DHDMIQK(KAP).

Targeting delivery of DHDMIQK(KAP) toward the thrombus

The targeting of DHDMIQK(KAP) is mirrored in its distribution and that of its moieties, and so FT-MS spectrum analysis of the extracts of homogenates of the thrombus, blood, brain, heart, liver, lung, kidney and spleen of the rats treated with NS and DHDMIQK(KAP) was performed.

Fig. 8A is a FT-MS spectrum of the thrombus extract of the rats treated with DHDMIQK(KAP), which is recorded in positive ion mode and gives an ion peak at 662.38716 of the mass of the DHDMIQK(KAP) molecule plus H. Fig. 8A also gives an ion peak at 443.30275 of the mass of KPAK plus H. Fig. 8B is a FT-MS spectrum of the thrombus extract of the rats treated with DHDMIQK(KAP), which is recorded in negative ion mode and gives an anion peak at 236.09264 of the mass of DHDMIQ minus H. The two FT-MS spectra clarify that DHDMIQK(KAP), DHDMIQ and KPAK are found in the thrombus.

Fig. 8C and D are the FT-MS spectra of the blood extract of the rats treated with DHDMIQK(KAP), which are recorded in positive and negative ion modes, respectively, and do not give the same ion and anion peaks as those of Fig. 8A and B, suggesting no DHDMIQK(KAP), DHDMIQ and KPAK could be found in the blood extract of the rats.

It is worthy of mention that the FT-MS spectra of the extracts of the homogenates of the brain, heart, liver, lung, kidney and

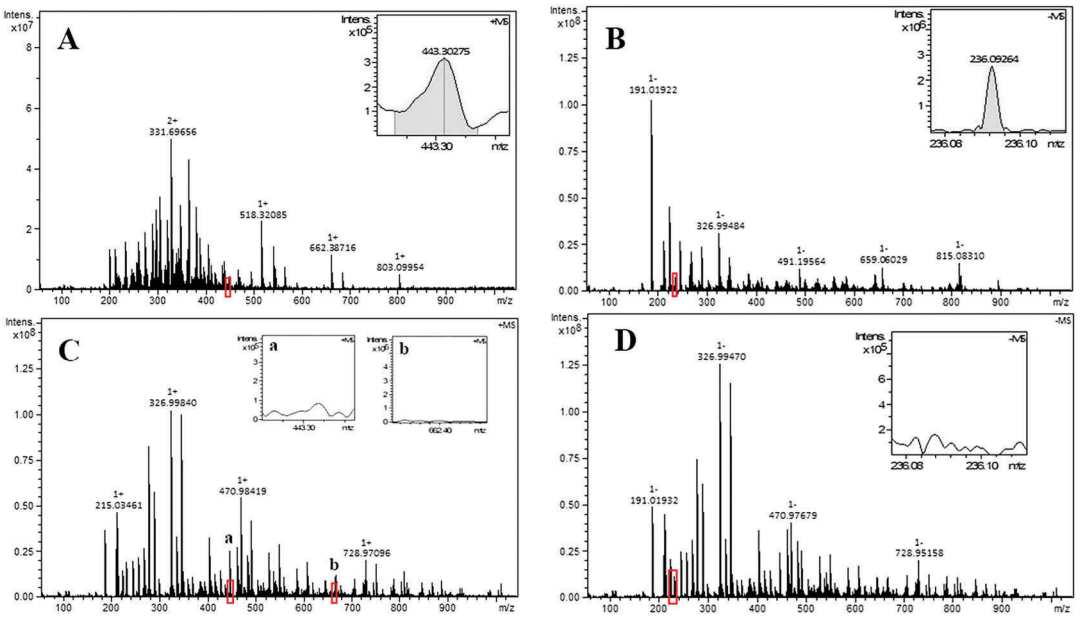

Fig. 8 FT-MS spectra of the thrombus and blood extracts of the rats treated with DHDMIQK(KAP). (A) FT-MS spectrum of the thrombus extract and the amplified ion peaks of DHDMIQK(KAP) and KPAK, in which the inset represents the amplified peak of KPAK at 443.30275; (B) FT-MS spectrum of the thrombus extract and the amplified anion peak of DHDMIQ, in which the inset represents the amplified peak of DHDMIQ at 236.09264; (C) FT-MS spectrum of the blood extract dual ion source in positive ion mode, the insets show no any interest peaks could be found at 443 and 662; (D) FT-MS spectrum of the blood extract in negative ion mode, the inset shows no any interested peak could be found at 236.

spleen of the rats treated with DHDMIQK(KAP) also do not give the same ion and anion peaks as those of Fig. 8A and B (see Fig. S7A and B of ESI†), again suggesting that no DHDMIQK(KAP), DHDMIQ and KPAK could be found in the brain, heart, liver, lung, kidney and spleen of the rats.

Therefore, the FT-MS spectrum analyses of the extracts of the homogenates of the thrombus, blood, brain, heart, liver, lung, kidney and spleen of the rats treated with DHDMIQK(KAP) identify that after the administration DHDMIQK(KAP), DHDMIQ and KPAK only exist in the thrombus, but not in the blood and the vital organs. This means that DHDMIQK(KAP) is a thrombus targeting nano-delivery system. In the thrombus, DHDMIQK(KAP) acts either in the form of the whole molecule or in the form of its metabolites DHDMIQ and KPAK.

AFM images evidencing the adhesion of DHDMIQK(KAP) nanoparticles on platelets

We hypothesized that adhesion on the surfaces of platelets is a key step of DHDMIQK(KAP)'s activity as an anti-thrombotic and thrombolytic agent. Compared to the molecule alone, nanoparticles should benefit the adhesion, and thereby improve the anti-thrombotic and thrombolytic activities. To visualize the superiority of the nanoparticles over the molecule alone in adhesion on the surfaces of the platelets, AFM images of resting rat platelets in NS, resting rat platelets with 10^{-7} M of DHDMIQK(KAP) solution, AA-activated rat platelets in NS, and AA-activated rat platelets with 10^{-7} M of DHDMIQK(KAP) solution were recorded and are shown in Fig. 9. Fig. 9A indicates that the surfaces of the resting rat platelets are relatively smooth. Fig. 9B indicates that when the resting rat platelets are treated with 10^{-7} M of DHDMIQK(KAP)

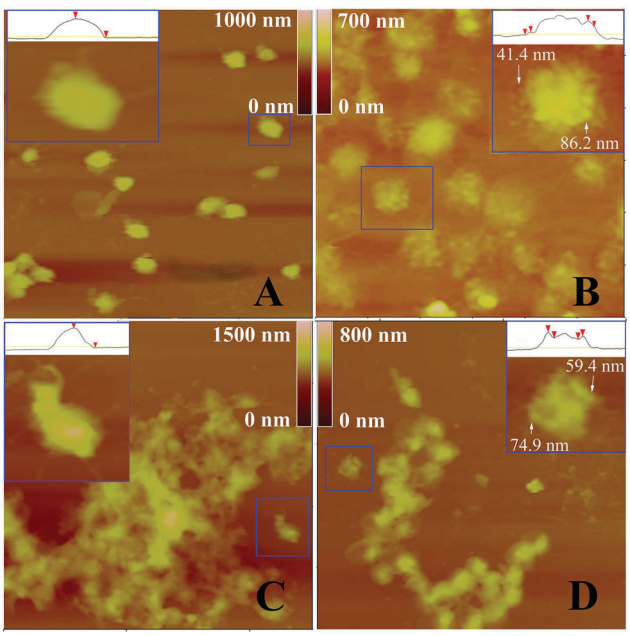

Fig. 9 AFM images of resting rat platelets, the inset amplifies and shows the resting rat platelet having smooth surfaces (A), resting rat platelets with 10^{-7} M of DHDMIQK(KAP) solution, the inset amplifies and shows on the surface of the rat platelet there are numerous nanoparticles of 40–80 nm in diameter (B), AA-activated rat platelets, the inset amplifies and shows that the platelets extend their pseudopodia to form aggregators, but the surfaces are still relatively smooth (C), and AA-activated rat platelets with 10^{-7} M of DHDMIQK(KAP) solution, the inset amplifies and shows that on the surfaces of the rat platelets there are numerous nanoparticles of ~60–75 nm in diameter, but no pseudopodia (D).

solution there are numerous nanoparticles of ~40–80 nm in diameter on the surfaces of the rat platelets. Fig. 9C indicates that when the resting rat platelets are treated with AA, the platelets extend their pseudopodia to form aggregators, but the surfaces are still relatively smooth. Fig. 9D indicates that when AA-activated platelets are treated with 10^{-7} M of DHDMIQK(KAP) solution there are numerous nanoparticles of ~60–75 nm in diameter on the surfaces of the rat platelets. These comparisons of the AFM images evidence that the nanoparticles of DHDMIQK(KAP) are capable of adhering onto the surfaces of both resting rat platelets and AA-activated rat platelets, and confirm the abovementioned hypothesis.

Conclusions

A P-selectin enzyme-linked immunosorbent experiment confirms that P-selectin active pocket docking based computer screening rationally leads to the discovery of DHDMIQK(KAP) as a novel P-selectin inhibitor. TEM, SEM and AFM images confirm that mesoscale simulation also rationally leads to the discovery of DHDMIQK(KAP) as a nanoscale P-selectin inhibitor. FT-MS, NOESY 2D ^{1}H NMR and free energy optimization together show that through intermolecular interactions DHDMIQK(KAP) forms hexamers of a butterfly-like conformation and forms size-suitable nanoparticles for safe delivery in the blood circulation. *In vitro* DHDMIQK(KAP) effectively inhibits platelet aggregations induced by TH, AA, ADP and PAF, which are correlated with the down-regulation of P-selectin expression and with the scavenging of the free radicals. *In vivo* DHDMIQK(KAP) dose dependently inhibits thrombosis and lyses thrombi, the minimal effective dose is as low as 0.01 nmol kg^{-1}. At this dose the thrombolytic and anti-thrombotic activities of DHDMIQK(KAP) are 10 fold higher than those of 20 000 UI kg^{-1} of UK and 16.7 μmol kg^{-1} of aspirin. The 0.01 nmol kg^{-1} minimal effective thrombolytic and anti-thrombotic dose *in vivo* could be due to the nanoparticles of DHDMIQK(KAP) effectively adhering onto the surfaces of the platelets and their safe delivery in the blood circulation, as well as DHDMIQK(KAP) targeting the thrombus.

Acknowledgements

The authors thank the BMSTC (Z141100002114049), TJSHG (201310025008), KZ201610025029, the Project of Construction of Innovative Teams and Teacher Career Development for Universities and Colleges under Beijing Municipality, NSFC (81270046, 81273379, 81373264 and 81373265), BNSF (7162025) and 863 program (AA2015020902) for financial support.

Notes and references

1 H. Jin, M. A. Gebska, I. O. Blokhin, K. M. Wilson, P. Ketsawatsomkron, A. K. Chauhan, H. L. Keen, C. D. Sigmund and S. R. Lentz, *Arterioscler., Thromb., Vasc. Biol.*, 2015, **35**, 838–844.
2 A. T. Nurden, *Thromb. Haemostasis*, 2011, **105**, S13–S33.
3 A. Polek, W. Sobiczewski and J. Matowicka-Karna, *Postepy Hig. Med. Dosw.*, 2009, **63**, 465–470.
4 Z. M. Dong, A. A. Brown and D. D. Wagner, *Circulation*, 2000, **101**, 2290–2295.
5 P. M. Ridker, J. E. Buring and N. Rifai, *Circulation*, 2001, **103**, 491–495.
6 E. Folch, A. Salas, N. Prats, J. Panés, J. M. Pioué, E. Gelpí, J. Roselló-Catafau and D. Closa, *Free Radicals Biol. Med.*, 2000, **28**, 1286–1294.
7 R. Chelliah, A. J. Lucking, L. Tattersall, S. Daga, N. J. Beresford-Cleary, K. Cortas, K. A. A. Fox, G. Z. Feuerstein, T. M. Connolly and D. E. Newby, *J. Thromb. Haemostasis*, 2009, **7**, 1915–1919.
8 C. V. Gomes, M. P. Kaster, A. R. Tome, P. M. Agostinho and R. A. Cunha, *Biochim. Biophys. Acta*, 2011, **1808**, 1380–1399.
9 P. Popoli, D. Blum, M. R. Domenici, S. Burnouf and Y. Chern, *Curr. Pharm. Des.*, 2008, **14**, 1500–1511.
10 D. Preti, P. G. Baraldi, A. R. Moorman, P. A. Borea and K. Varani, *Med. Res. Rev.*, 2015, **35**, 790–848.
11 V. Moas-Héloire, N. Renault, V. Batalha, A. R. Arias, M. Marchivie, S. Yous, N. Deguine, L. Buée, P. Chavatte, D. Blum, L. Lopes, P. Melnyk and L. Agouridas, *Eur. J. Med. Chem.*, 2015, **106**, 15–25.
12 D. Chen, A. Shen, G. Fang, H. Liu, M. Zhang, S. Tang, B. Xiong, L. Ma, M. Geng and J. Shen, *Acta Pharm. Sin. B*, 2016, **6**, 93–99.
13 R. Achary, J. I. Yun, C. M. Park, G. R. Mathi, J. Y. Lee, J. D. Ha, C. H. Chae, S. Ahn, C. H. Park, C. O. Lee, J. Y. Hwang, C.-S. Yun, H. J. Jung, S. Y. Cho, H. R. Kim and P. Kim, *Bioorg. Med. Chem.*, 2016, **24**, 207–219.
14 G. Song, D. Zhao, D. Hu, Y. Li, H. Jin and Z. Cui, *Bioorg. Med. Chem. Lett.*, 2015, **25**, 4610–4614.
15 J. J. Swidorski, Z. Liu, Z Yin, T. Wang, D. J. Carini, S. Rahematpura, M. Zheng, K. Johnson, S. Zhang, P.-F. Lin, D. D. Parker, W. Li, N. A. Meanwell, L. G. Hamann and A. Regueiro-Ren, *Bioorg. Med. Chem. Lett.*, 2016, **26**, 160–167.
16 H. J. Son, S. H. Han, J. A. Lee, C. S. Lee, J. W. Seo, D. Y. Chi and O. Hwang, *Eur. J. Pharmacol.*, 2016, **771**, 152–161.
17 J. Kitanaka, N. Kitanaka, F. S. Hall, G. R. Uhl, H. Asano, R. Chatani, S. Hayata, H. Yokoyama, K.-I. Tanaka, N. Nishiyama and M. Takemura, *Brain Res.*, 2012, **1439**, 15–26.
18 M. Zhong, W. Shen, K. J. Barr, J. P. Arbitrario, M. R. Arkin, M. Bui, T. Chen, B. C. Cunningham, M. J. Evanchik, E. J. Hanan, U. Hoch, K. Huen, J. Hyde, J. L. Kumer, T. Lac, C. E. Lawrence, J. R. Martell, J. D. Oslob, K. Paulvannan, S. Prabhu, J. A. Silverman, J. Wright, C. H. Yu, J. Zhu and W. M. Flanagan, *Bioorg. Med. Chem. Lett.*, 2010, **20**, 5269–5273.
19 D. A. Perrey, A. M. Decker, J.-X. Li, B. P. Gilmour, B. F. Thomas, D. L. Harris, S. P. Runyon and Y. Zhang, *Bioorg. Med. Chem.*, 2015, **23**, 5709–5724.
20 K. J. Frankowski, S. R. Slauson, K. M. Lovell, A. M. Phillips, J. M. Streicher, L. Zhou, D. A. Whipple, F. J. Schoenen, T. E. Prisinzano, L. M. Bohn and J. Aubé, *Bioorg. Med. Chem.*, 2015, **23**, 3948–3956.
21 T. Ogiyama, M. Inoue, S. Honda, H. Yamada, T. Watanabe, T. Gotoh, T. Kiso, A. Koakutsu, S. Kakimoto and J.-I. Shishikura, *Bioorg. Med. Chem.*, 2015, **23**, 6079.

22 S. Kotha, D. Deodhar and P. Khedkar, *Org. Biomol. Chem.*, 2014, **12**, 9054–9091.
23 M. Zheng, X. Zhang, M. Zhao, H. W. Chang, W. Wang, Y. Wang and S. Peng, *Bioorg. Med. Chem.*, 2008, **16**, 9574–9587.
24 G. Yang, H. Zhu, M. Zhao, J. Wu, Y. Wang, Y. Wang, M. Zheng, M. Chen, J. Liu and S. Peng, *Mol. BioSyst.*, 2012, **8**, 2672–2679.
25 A. Wąsik, E. Możdżeń, I. Romańska, J. Michaluk and L. Antkiewicz-Michaluk, *Eur. J. Pharmacol.*, 2013, **700**, 110–117.
26 R. J. Nijveldt, E. van Nood, D. E. van Hoorn, P. G. Boelens, K. van Norren and P. A. van Leeuwen, *Am. J. Clin. Nutr.*, 2001, **74**, 418–425.
27 M. Yang, G. Cui, M. Zhao, C. Wang, L. Wang, H. Liu and S. Peng, *Int. J. Pharm.*, 2008, **362**, 81–87.
28 R. U. Palekar, J. W. Myerson, P. H. Schlesinger, J. E. Sadler, H. Pan and S. A. Wickline, *Mol. Pharmaceutics*, 2013, **10**, 4168–4175.
29 J. Myerson, L. He, G. Lanza, D. Tollefsen and S. Wickline, *J. Thromb. Haemostasis*, 2011, **9**, 1292–1300.
30 D. Peters, M. Kastantin, V. R. Kotamraju, P. P. Karmali, K. Gujraty, M. Tirrell and E. Ruoslahti, *Proc. Natl. Acad. Sci. U. S. A.*, 2009, **106**, 9815–9819.
31 H. Zhu, Y. Wang, M. Zhao, J. Wu, X. Zhang, G. Yang and S. Peng, *MedChemComm*, 2013, **4**, 1066–1072.
32 Y. Fujita, M. Mie and E. Kobatake, *Biomaterials*, 2009, **30**, 3450–3457.
33 C. Skoglund, J. Wetterö, P. Tengvall and T. Bengtsson, *Immunobiology*, 2010, **215**, 987–995.
34 E. Folch, A. Salas, N. Prats, J. Panés, J. M. Pioué, E. Gelpí, J. Roselló-Catafau and D. Closa, *Free Radicals Biol. Med.*, 2000, **28**, 1286–1294.
35 H. Kolarova, A. Klinke, S. Kremserova, M. Adam, M. Pekarova, S. Baldus, J. P. Eiserich and L. Kubala, *Free Radicals Biol. Med.*, 2013, **61**, 357–369.
36 M. Yang, G. Cui, M. Zhao, C. Wang, L. Wang, H. Liu and S. Peng, *Int. J. Pharm.*, 2008, **362**, 81–87.
37 A. K. Srivastava, J. Kalita, P. Dohare, M. Ray and U. K. Misra, *Neurosci. Lett.*, 2009, **450**, 127–131.
38 G. R. Nigri, S. Kossodo, P. Waterman, P. Fungaloi and G. M. LaMuraglia, *J. Vasc. Surg.*, 2004, **39**, 843–849.
39 E. Ramacciotti, D. D. Myers Jr., S. K. Wrobleski, K. B. Deatrick, F. J. Londy, J. E. Rectenwald, P. K. Henke, R. G. Schaub and T. W. Wakefield, *Thromb. Res.*, 2010, **125**, e138–e142.